Evolution of Anode Porosity under Air Oxidation: The Unveiling of the Active Pore Size

FrancoisChevarin[1], Ramzi Ishak[2], Donald Ziegler[3], Mario Fafard[4] and Houshang Alamdari[5]

1. Professional researcher
2. Ph.D. student
5. Professor

Department of Mining, Metallurgical and Materials Engineering,
Université Laval, Québec, Canada
NSERC/Alcoa Industrial Research Chair MACE[3] and Aluminum Research Centre – REGAL
Université Laval, Québec, Canada

3. Carbon manager

[3]Alcoa Primary Metals, Alcoa Technical Center, PA, USA

4. Professor

NSERC/Alcoa Industrial Research Chair MACE[3] and Aluminum Research Centre – REGAL
Université Laval, Québec, Canada
Corresponding author: houshang.alamdari@gmn.ulaval.ca

Abstract

Carbon anode, used in the aluminum electrolysis (Hall-Héroult process) is overconsumed by air oxidation. Several anode features may affect this overconsumption such as the impurity content, the graphitization level and the anode porosity (e.g. apparent density, porosity, pore size distribution). The two first parameters are basically related to the quality of the raw materials and the coke calcination conditions. The anode porosityis however affected by the anode manufacturing conditions, thus possible to be modified, to some extent, by adjusting the anode recipe and the processing parameters. This work aims at investigating the effect of anode porosityon its air reactivity. The porosity was characterized in several pore size ranges, measured by mercury porosimetry. Anode samples, in particle form, were then gasified at different levels under air at 525°C. The volume variation of each pore range versus carbon conversion was assessed and used to determine the size of the most active pores for air oxidation. Limitation of this pore size range could be used as an additional guideline, along with other targets such as high homogeneity and density, to set the optimum anode manufacturing parameters.

Keywords: Air reactivity; pore size distribution; active pore size; apparent density; gasification.

1 Introduction

Aluminum is produced by the reduction of alumina (Al_2O_3) in an electrolysis cell at 960°C according to the Hall-Héroult process. The cell is made of carbon anodes, carbon cathode and molten cryolite as electrolyte. The carbon anode is composed of calcined petroleum coke, used anodes (butts) and coal tar pitch. In the electrolysis cell, the anode top is exposed to the ambient air (despite a covering of crushed bath and alumina) and the temperature is comprised between 400 and 600 °C [1]. In this range, the oxygen of the air can react with the carbon anode, according to the Equations 2. Both reactions are undesirable since the carbon anode is consumed without producing metal. Between 8 and 30% of anode is consumed by the air oxidation (according to the anode quality and the cell conditions)[2].

$$C\ (anode) + O_2\ (g) \rightarrow CO_2\ (g) \quad (2a)$$
$$2\ C\ (anode) + O_2\ (g) \rightarrow 2\ CO\ (g) \quad (2b)$$

Several studies have been published to reveal the essential parameters controlling the air oxidation. The air reactivity is correlated with different parameters i.e. the raw material properties such as the calcination level of coke [3-5], the level of anode impurities [6-9] and the air reactivity of the coke[10], or the manufacturing steps of the anode, for instance, the temperature and the soaking time during anode baking [11-15] and the anode recipe [16, 17]. Some studies also reported the effect of the operation conditions in the cell, i.e. the temperature of the anode top, the protection effect of alumina covering [1, 18] and the current density[19].

Most of these parameters are controlled by the quality of the raw materials. Edwards [20] detailed the deterioration of the coke quality and the new challenges of the aluminum smelters to keep a good quality of anodes. To decrease the air oxidation, the anode manufacturing steps could be considered to counterbalance the poor properties of raw materials. Tkac [21] proposed that some parameters such as the interaction of the pitch content, the mixing time of raw materials and the applied pressure during vibrocompation influence the air reactivity. These parameters could influence the anode oxidation because they may increase the anode porosity and favor air burning.

Suriyapraphadilok et al.[22]and Bird et al. [23] remarked that the interior of anode changed with the air gasification leading to pore volume variations. Turkdogan [24] proposed that the pores larger than a micron in carbon material control the air reactivity. For coke materials, the active pore range seems to be comprised between 0.5 and 15 µm [5]. In the same way, Tran et al. [25]found that the volume of the three pore size ranges (inferior to 2 nm, between 2 and 50 nm and superior to 50 nm) increased with the gasification percentage. Tordai [26] revealed that the anode air burning takes place preferentially in the pores comprised between 1 and 10 µm. Chevarin et al. [27] proposed that the air reactivity of industrial carbon anode could be controlled by the pores with a pore entrance radius of 1.5 and 12 µm. The porosity thus seems to have a significant effect on the air reactivity of anode material. However, the weight of each pore size during the anode gasification was not clearly quantified. In this work, the authors try to reveal the role of porosity and external surface of particles in gasification of carbon anodes.

2 Experimental procedure

2.1 Materials

Prebaked anodes at laboratory scale were prepared following atypical recipe used in the anode manufacturing process. The raw materials used in this work were provided by Deschambault aluminium smelting plant (Alcoa, Canada). The anode recipe comprised calcined coke (86.1 wt.%) and coal tar pitch (13.9 wt.%) (Table 1).Fractions of the coke particle are detailed in Table 2. The coke particles were preheated at 185 °C for 90 minutes admixed with the pitch. The blend was mixed at the same temperature for 10 minutes and then pressed at 150 °C during 3 minutes by applying a uniaxial pressure of 70 MPa [28-30]. This sample, called green anode, had a diameter of 50 mm and an approximate height of 100 mm. prior to baking in a muffle furnace, the green samples were placed in an Inconel® box and covered by coke particles in order to protect them against air oxidation. The heating program was as follows: from room temperature to 150 °C at a heating rate of 60 °C/h, then from 150 °C to 650 °C at a rate of 20 °C/h, and finally from 650 °C to 1100 °C at a rate of 50 °C/h. This was followed by a soaking time of 20 hours at 1100 °C. At the end of this cycle, the furnace was switched off and allowed to cool to room temperature. The anode samples were thereafter crushed using jaw and roll crushers and sieved through two different USA standard sieve trays, which were chosen in order to get a narrow particle size range of 4000 to 4380 µm(- 4 + 5 US Mesh). The particle size range

corresponds to the largest particle size which could be characterized by the analytical instruments used in this study. The anode particles properties are detailed in Table 3.

Table 1. Chemical composition of calcined coke and coal tar pitch.

Properties	S (%)	Na (ppm)	Si (ppm)	Ca (ppm)	V (ppm)	Fe (ppm)	Ni (ppm)
Calcined coke	2.13 ± 0.06	100 ± 7	120 ± 17	130 ± 7	360 ± 18	460 ± 23	250 ± 13
Coal tar pitch	0.55 ± 0.02	48 ± 3	254 ± 36	71 ± 4	N/A	209 ± 10	N/A

Table 2. Particle size distribution of calcined coke (wt.%) used for the preparation of the dry mixture used for the fabrication of prebaked anodes.

Particle sizes (US Mesh)	- 4 + 8	- 8 + 16	- 16 + 30	- 30 + 50	- 50 + 100	- 100 + 200	Fines (4000 Blaine Number)
Particle sizes (µm)	-4760 2380	-2380 1410	-1410 595	-595 297	-297 149	-149 74	149>
Coke (wt.%)	22.0	10.0	11.5	12.7	8.8	10.8	24.2

Table 3. Sample properties of the particles of baked anode.

Properties	S (%)	Na (ppm)	Si (ppm)	Ca (ppm)	V (ppm)	Fe (ppm)	Ni (ppm)	L_C (nm)	Particle weight (mg)
Anode	1.81 ± 0.05	650 ± 91	624 ± 31	377 ± 19	224 ± 11	119 ± 8	341 ± 17	2.9 ± 0.1	73.2 ± 22.0

2.2 Air reactivity tests

Two air reactivity tests were performed: the Thermo-Gravimetric Analysis with an analytical balance (TGA) and a Fixed Bed Reactor (FBR). TGA has been used in order to estimate the apparent reaction rate, r (Equation 3) of the anode particles by measuring the sample weight loss for a defined interval of time (0–7 hours) at 525 °C, according to the standard ISO 12989-2.Aquartzcrucible was used for all TGA measurements. 50 to 300 mg of anode particles (corresponding to 1 to 3 particles) were gasified under air atmosphere[31, 32]. Five gasification tests were performed and the reaction rate was determined using equation (3)

$$r = -\frac{1}{m(t)} \times \frac{dm}{dt} = -\frac{1}{(1-X)} \times \frac{dX}{dt} \quad (3)$$

Where: *m(t)*: instantaneous mass at time t
dm: mass loss in the time interval dt
X: carbon conversion at time t

Since the quantity of the samples used in TGA was too small for analytical instruments, larger amounts of material were gasified in the FBR for further characterizations. A similar methodology was used by Chevarin et al. [33, 34]. Between 10 and 40 anode particles (1 to 3 g) were placed in a monolayer (to limit the inter-particular mass transport) in an alumina tray and put in the FBR. The materials were heated under inert atmosphere (N_2 gas) until the target temperature is reached. The sample was gasified under air at a similar temperature as TGA at different reaction times (between 1 and 4 hours). After a specific duration of carbon conversion, the furnace was switched off and the anode particles were cooled down under inert atmosphere.

To quantify the dusting during the anode oxidation, the gasified carbon particles were sieved through one USA standard sieve (8 US Mesh, 2380 µm). Considering the maximum gasification percentage studied in this work (50% of gasification corresponding to half of the upper limit of the initial particle size), a sieving after gasification could reveal the portions of the residue i.e. the residual body of the anode particles superior to2380 µm, the dust (broken particles and fines particles with a size inferior at 2380 µm), and the mass loss corresponding tothe combustion of carbon particles with gas species (CO_2 and CO molecules) (ISO 12989).

2.3 Analytical instruments

The crystallite size (L_C) and the level of impurities were measured by XRD (Phillips, PW 1800 with the ISO standard 20203) and XRF (PANalytical Axios max according to the ASTM D4326-06 standard) spectrometers, respectively. The helium density of the anode particles was measured by a Helium-Pycnometer (Micromeritics, AccuPyc II 1340). Each sample of about 50 g was weighed by an analytical balance (MS204S, Mettler Toledo) and put in the 100 cm^3 stainless steel cell of the He-Pycnometer. The helium molecules can penetrate the submicron pores ranging down to 0.3 nm [35] in order to measure the volume of the material excluding the pore volume.

The specific surface area, pore volume and pore size distribution of anode particles were measured by two different techniques[36]:

- Between 0.0014 and 0.100 µm of pore size, a gas adsorption analyzer (Micromeritics, Tristar II 3020) with the Density Functional Theory (DFT) equation and the nitrogen adsorptive gas was used;
- For the pores superior at 0.1 µm until about 1 000 µm (ISO 15901-1), a mercury porosimeter (Micromeritics, Auto Pore IV) was used.

3 Results and discussion

3.1 TG Analysis

To estimate the air reactivity, the anode particles were gasified in the TG instrument at 525°C, under air atmosphere. The apparent reaction rate of anode particles as a function of carbon conversion is presented in Figure 1.The rate of reaction increased gradually between 0 and 70% of gasification and decreased between 70 and 80%. This trend of apparent reaction rate exhibiting a maximum has often been remarked for carbon consumption in the literature[25, 37-40].Bhatia and Perlmutter[39] and Ballal and Zygouraki [40]explained the maximum rate with the combination of two opposite effects: the augmentation of the reactive surface with the pore growth and the pore accessibility, and the disappearance of this surface area with the pore coalescence and the consumption of carbon material.

To reveal the evolution of the anode porosity as a function of carbon conversion, a structural analysis is required. However, as reported previously, the TG instrument allows gasifying only a small quantity of material. Thus, a second reactor is necessary to have enough materials for characterisation.

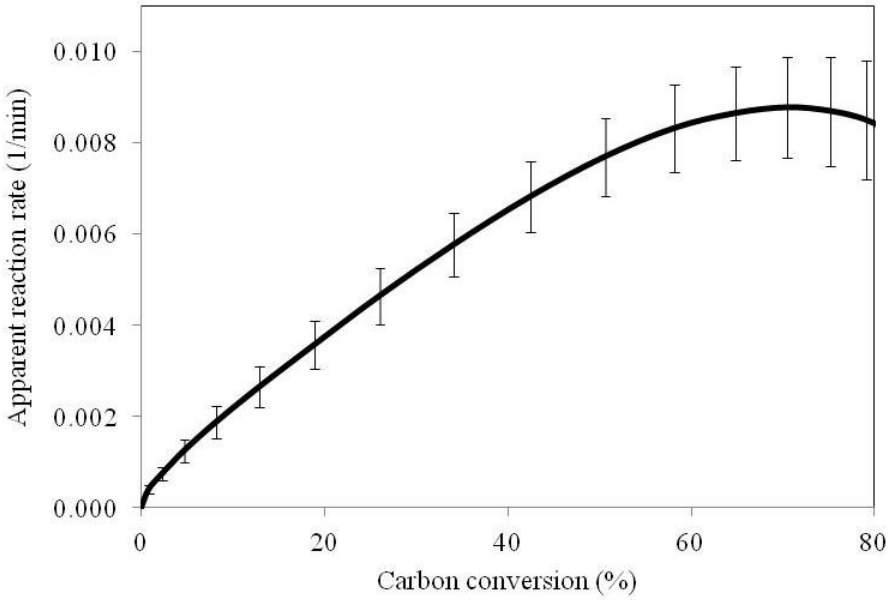

Figure 1. Apparent reaction rate of the anode particles (- 4760 + 4000 µm) as a function of carbon conversion at 525°C, under air atmosphere; analyses performed on a TGA instrument.

3.2 Fixed Bed Reactor gasification

To obtain a large amount of gasified materials, a Fixed Bed Reactor (FBR) was used. After a specific reaction time, the anode particles were sieved to reveal the portions of residue, dust and mass loss in the form of CO_2 and CO. Figure 2 presents these for the anode particles gasified during 1; 2; 2.5; 3 and 4 hours under air at 525 °C. Although the mass loss of the residue decreases with increasing reaction time, the weight lost of dust and the loss were increased. Figure. 2 compares the importance of carbon loss into gas against the dust loss.

After sieving of the gasified materials in FBR, some analyses were performed on the residues to characterise the attacked materials, to reveal the most important parameter controlling the reactivity, and to understand the augmentation of the reaction rate.

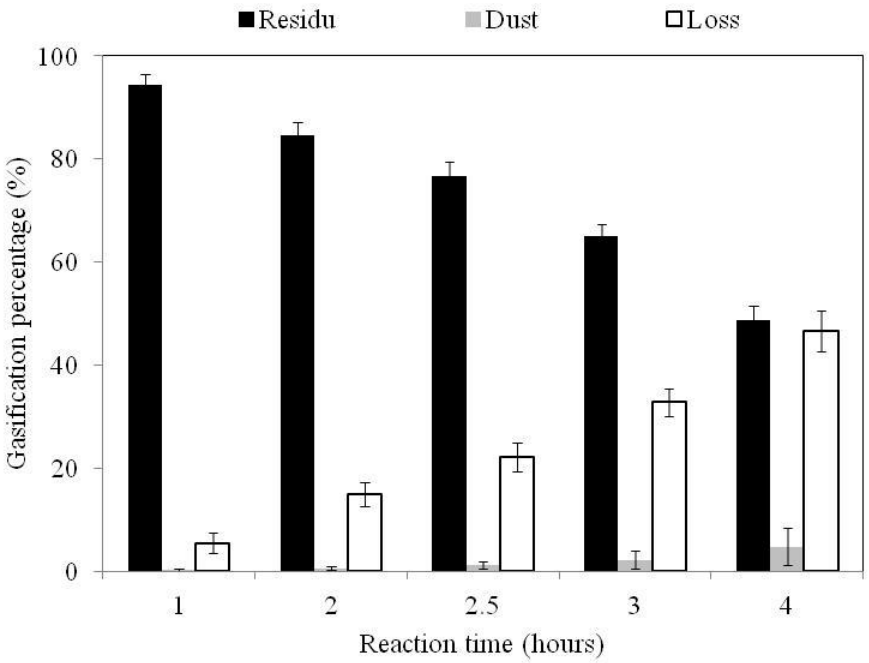

Figure 2. Portions of residue, dust and loss of anode particles gasified for 5 times (1; 2; 2.5; 3 and 4 hours) under air atmosphere at 525°C; analyses performed on a Fixed Bed Reactor.

3.3 Density evolution during gasification

The helium density can be measured by He-pycnometer for semi-graphitic materials. Figure 3 presents the He-density evolution of the gasified anode particles, i.e. the residues (between 0 and 50%) under air at 525 °C in FBR. An augmentation of the helium density with an increase of carbon conversion from 0 to 35% and a plateau between 35 and 50% could be observed. Tran et al. [35]has shown that the gasification of anode particles with a size comprised between 180 and 212 µm shows an increase of helium density from 0 to 10% and a plateau between 10 and 70%. This discrepancy with the present study could be explained by the initial particle size (for the small particles, the closed pores have been probably opened by the sample preparation) and also by the different of raw materials. When the initial particle size is smaller, a large fraction of closed pores are opened at early stages of the gasification while it is delayed for the larger particles. Thus, the steady state of helium density is achieved faster in smaller particles.

Figure 1. has shown a quasi-linear increase of the reaction rate between 0 and 70%. In consequence, the variation of the helium density alone cannot explain this trend (not a plateau of reaction between 35 and 50%). Another structural parameter which can be considered, is the specific surface area according to the pore size distribution.

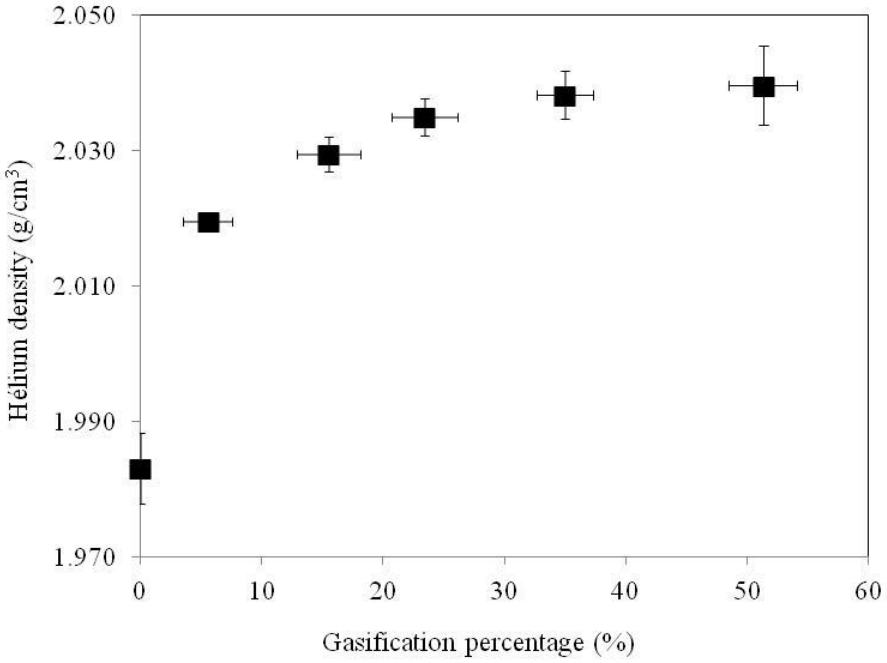

Figure 3. Helium density versus carbon conversion of the anode particles gasified at 5 levels (0; 5; 15; 25; 35 and 50%) under air at 525 °C.

3.4 Pore size and volume distribution

Figure 4 presents the pore volume distributions measured by liquid nitrogen using the DFT model (Figure 4-a) and by mercury intrusion (Figure 4-b) as a function of the pore size for anode particles gasified under air at 525 °C and at different gasification levels of 0, 5, 15, 25, 35 and 50%. In Figure 4-a, it is possible to distinguish three different pore size ranges: 0.0011-0.020; 0.002-0.025 and 0.025-0.100 µm. The mercury analysis (Figure 4-b) revealed two other pore size ranges: 0.1-40 µm and superior to 40 µm. The pore size limit of 40 µm could be denoted as the Critical Pore Size (CPS) because the mercury infiltration is not able to distinguish the large pores in the particles and the pores between the particles [41].After the determination of the experimental pore size ranges, it is possible to establish a relationship between the specific surface area in each pore size with the evolution of the apparent reaction rate.

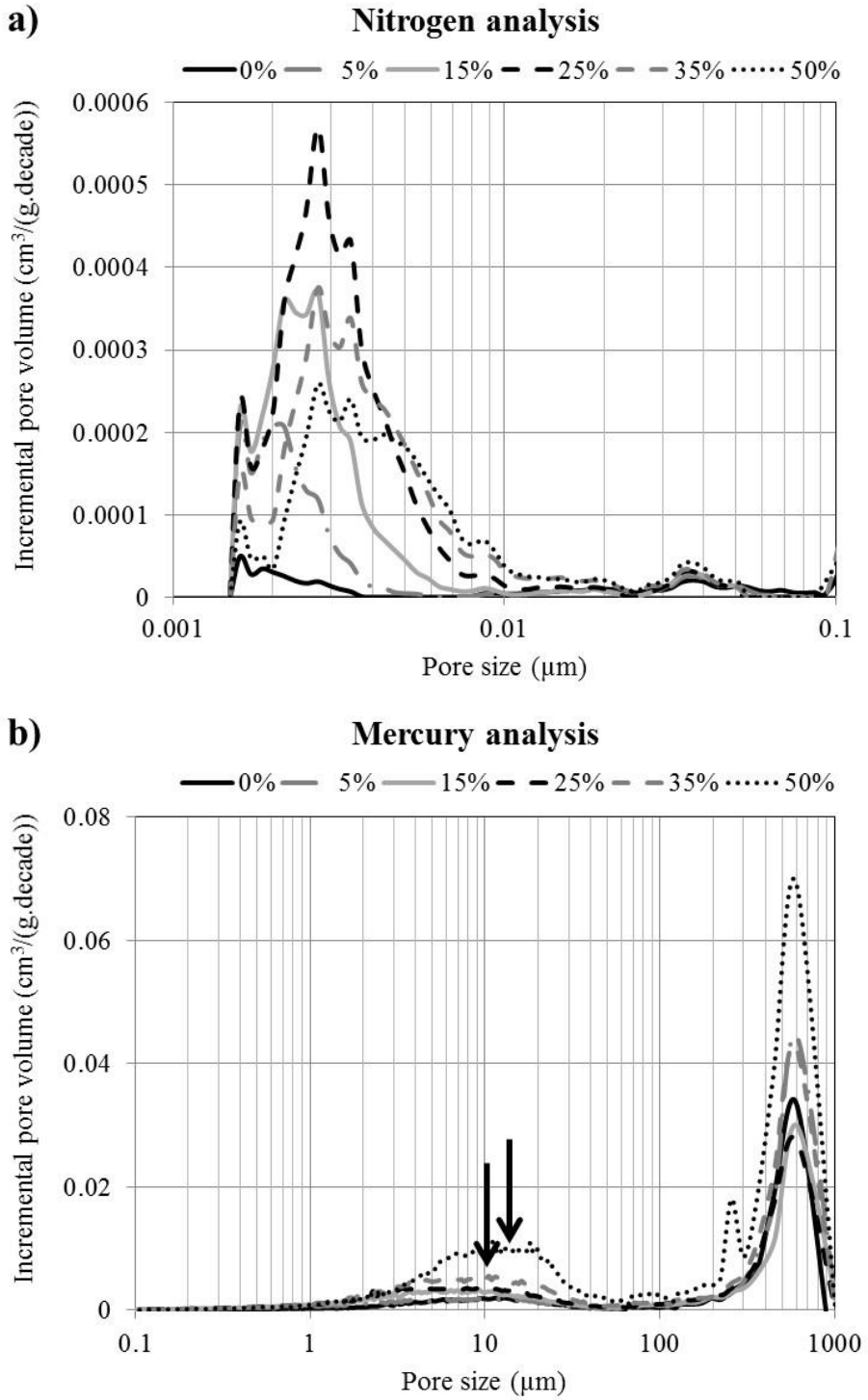

Figure 4. Pore volume distributions measured with liquid nitrogen using DFT model and with mercury intrusion versus the pore size diameter for anode particles gasified under air at 525 °C and at a rate of 0, 5, 15, 25, 35 and 50% in a fixed bed reactor.

3.5 Specific surface area

The carbon reactivity could be controlled by the level of impurities [2, 34, 42] and by the specific surface area [36, 43].Based on the BET model for the gas adsorption and with the assumption that the pores are cylindrical for the mercury analysis, it is possible to obtain the

specific surface area as a function of pore size distribution. This is shown in Figure 5 for anode particles, gasified at different five levels, measured with nitrogen adsorption (Figure 5-a) and mercury infiltration (Figure 5-b).

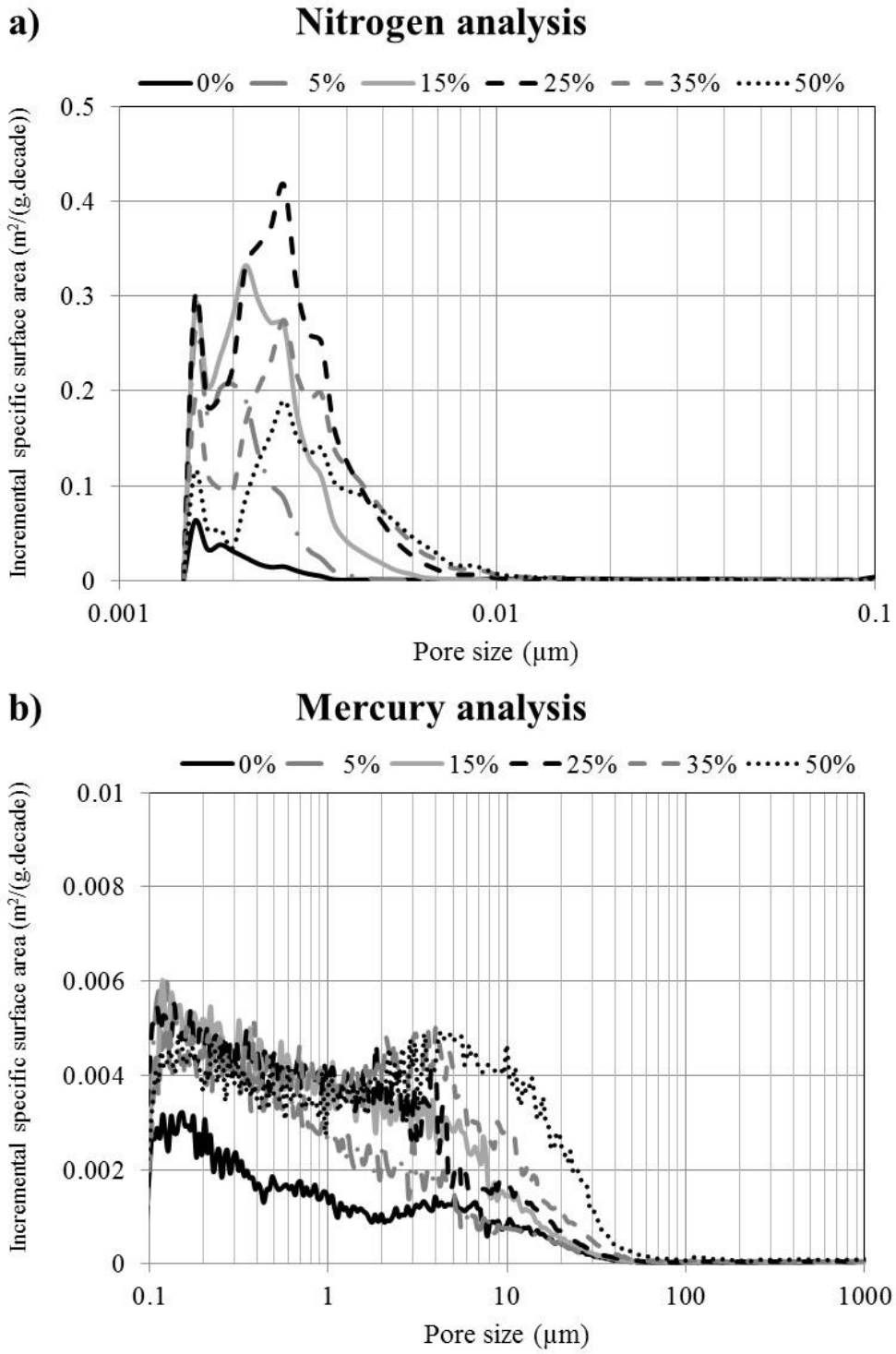

Figure 5. Specific surface areas measured with liquid nitrogen using DFT model and with mercury intrusion versus the pore size diameter for anode particles gasified under air at 525 °C and at a carbon conversion of 0, 5, 15, 25, 35 and 50% in a fixed bed reactor.

To reveal a possible relationship between the surface area and the variation of the apparent reaction rate (Figure 1), Figure 6 shows the cumulative specific surface area for each pore size range for the six gasification percentages of the anode particles. The specific surface area of the three smaller pore ranges (0.0014–0.002; 0.002–0.025 and 0.025–0.100 µm) presents a similar trend; an increase of the specific area following by a decrease of that one in function of the increasing of the carbon conversion. The two larger pore sizes (0.1–40 and superior at 40 µm) indicate a slight augmentation of the surface area as the reaction progresses. Thus, a possible correlation could be proposed between the increase of the surface areas in these two large pore ranges and the apparent reaction rate (Figure 1). In an objective to weigh the importance of each pore size, some calculations are performed to evaluate the carbon mass consumption in each pore size.

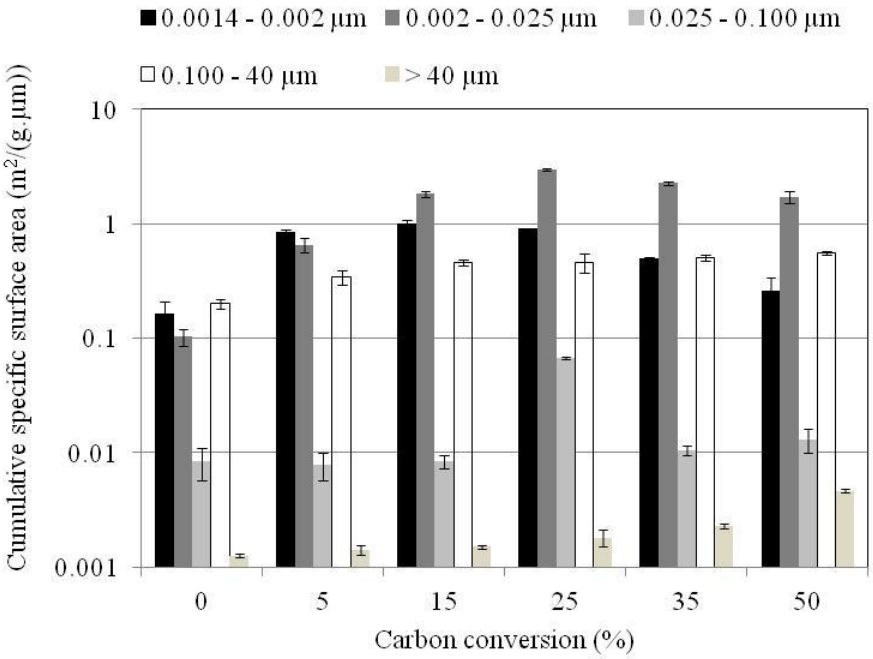

Figure 6. Cumulative specific surface area measured with liquid nitrogen using DFT mode and with mercury intrusion versus the pore size diameter for anode particles gasified at 0, 5, 15, 25, 35 and 50% under air at 525 °C in a fixed bed reactor.

3.6 Pore Volumes

Based on the pore volume distributions presented in Figure 4, a cumulative pore volume shows the variation of the pore volumes versus the carbon conversion of anode particles for the six levels of gasification under air at 525 °C (Figure 7). With nitrogen adsorption analysis, it is possible to reveal that the volume of the pores, in the range of 0.0014–0.002; 0.002–0.025 and 0.025–0.100 µm, presents a maximum with respect to carbon conversion, while the volume of pores in the range of 0.1-40 µm, measured with mercury infiltration, increases gradually with the gasification level. Thus, considering the progressive increase of the apparent reaction rate, it seems that the pores in the range of 0.1-40 µm control the gasification rate of the anode particles. The log scale of the Y-axis point out that the increase in the 0.1-40 range surpasses remarkably the increase of the other pore volumes. In an objective to confirm this hypothesis, it is essential to evaluate the amount of carbon consumption in different pore sizes as a function of carbon conversion.

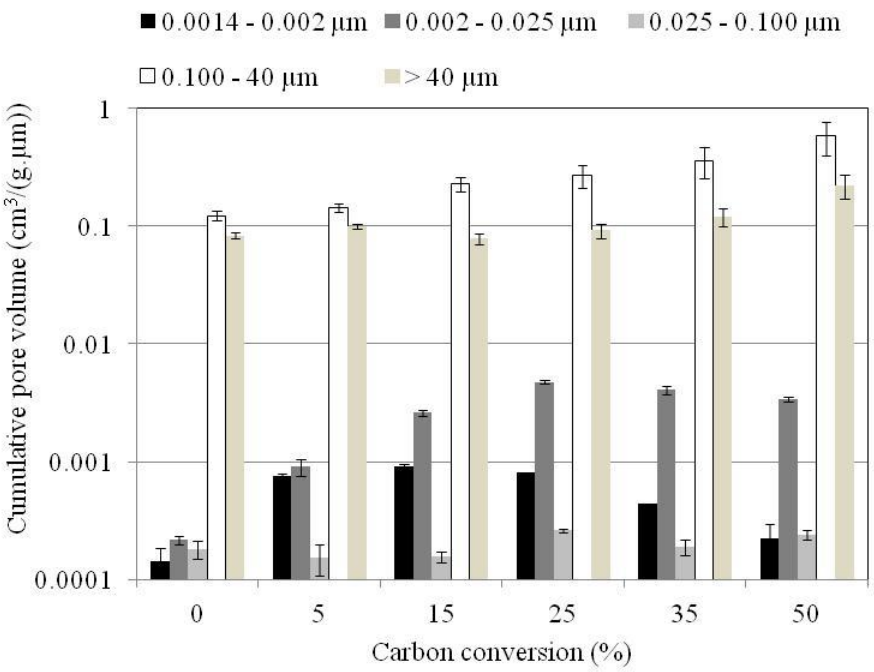

Figure 7. Cumulative pore volume measured with liquid nitrogen using DFT model (a) and with mercury intrusion (b) versus the pore size diameter for anode particles gasified at 0, 5, 15, 25, 35 and 50% under air at 525 °C in a fixed bed reactor.

3.7 Active pore size

In order to reveal the contribution of each pore size in gasified anode, the overall consumption is divided in two sub-classes, i.e. internal and external gasifications. The internal gasification is associated with the consumption in the material inside the pores smaller than 40 µm whereas the external gasification is attributed to the carbon consumption in the pores larger 40 µm. Then, the mass of the consumed carbon in each pore with a given size interval and at each gasification interval was evaluated. The detailed calculations were given in Chevarin et al. [44]. Figure 8illustrates the portions of external and internal contributions for five conversion ranges: 0–5, 5–15, 15–25, 25–35and 35–50%. Between 0 and 15% of conversion, the internal contribution (reaction in the pores smaller than 40 µm) controls the total gasification of anode, representing between 80 and 98% of the total conversion. After 15% of gasification, an inversion of the contribution type is observed. The external contribution (reaction in the pores larger than 40 µm) dominates preferentially the anode consumption, representing between 55 and 75% of the total gasification.

From 0 to 15% gasification, the pores smaller than 40 µm are enlarged (the average of the pore size is about 10 µm). At 15%, the pores with a size close to 40 µm (the average of the pore size shift to 20 µm), continue to grow and exceed the upper limit size. These pores shift to the larger pore size range and are considered the external pores. Thus, the contribution of these new large pores is added to the contribution of the initial large pores and increases the portion of the external contribution. The high reactivity of the large pores (0.1-40 µm) could be explained by an easier mass transport within these pores combined with the relatively large specific surface area. The contribution of the smaller pores, although exhibiting large specific surface area, is thus lower due to the mass transport limitations.

In consequence, the active pore size during carbon anode gasification under air is the pores with a size inferior to 40 µm and more specifically the size comprised between 0.1 and 40 µm because the volume variation of the pores inferior to 0.1 µm is very small (0.002 cm^3/g.decade)

versus 0.1 cm^3/g.decade for the range 0.1-40 µm).At the early steps of gasification (from 0 to 15%) the reaction essentially takes place in the small pores (0.1-40 µm). This step enlarges the pores and the pores superior to 40 µm become the active pores range between 15 and 50% of carbon conversion.

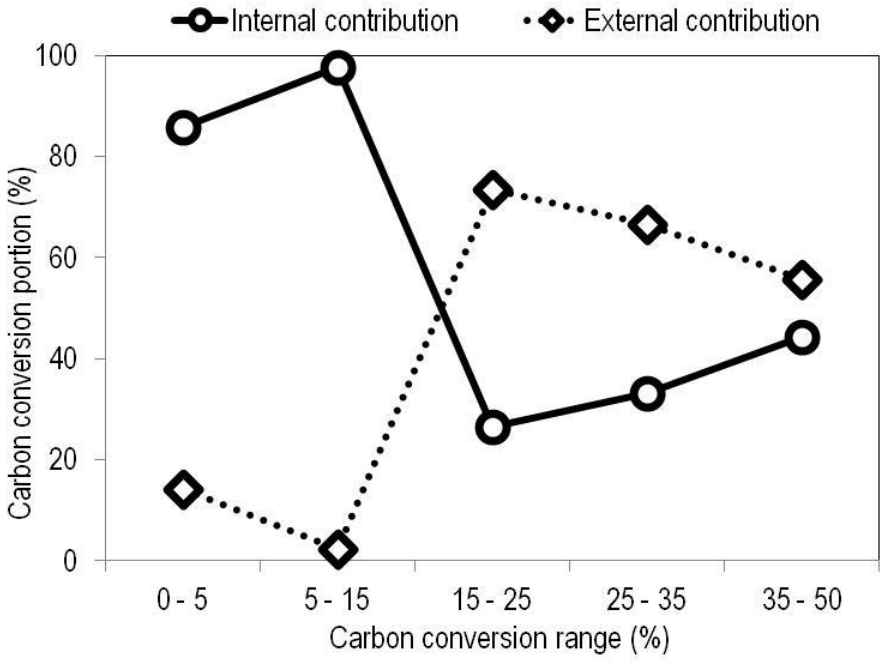

Figure 8. The weight of internal and external carbon contribution versus the carbon conversion ranges for anode particles gasified under air at 525 °C in a fixed bed reactor.

4 Conclusion

In the present study, anode particles were gasified under air at 525 °C in two different reactors (Thermogravimetric Analyzer and Fixed Bed Reactor) at six carbon conversions (0,5,15,25,35 and 50%). The consumed particles were sieved (to remove the dust) and their structural properties such as the He-density, specific surface areas and pore volumes have been characterized using several analytical instruments (He-pycnometer, gas adsorption analyzer, mercury porosimeter, etc.). The variation of gasification percentages of the anode particles allows us to evaluate the evolution of the surface area and the pore volumes for carbon conversion ranges.

Characterization of pore variation during gasification of anode particles under air revealed that the active pores are those with a size comprised between 0.1 and 40 µm. The important contribution of this pore size to the air gasification of the anode could be attributed to both high specific surface area and large pore volume providing less mass transport limitation.

5 Acknowledgments

The authors would like to acknowledge the financial support of Natural Sciences and Engineering Research Council of Canada, Fonds de Recherche du Québec - Nature et Technologies, Alcoa and the Aluminium Research Centre – REGAL. The assistance of Denis Drapeau and his colleagues at Alcoa Deschambault plant (QC, Canada) for conducting the chemical and crystallite size analyses is gratefully acknowledged. The authors would also like to extend their appreciation to Dr. Donald Picard at Laval University for the scientific discussions,

as well as Messrs. Jayson Tessier, Guillaume Gauvin and Hugues Ferland for their technical support.

6 References

1. Fischer, W.K. and R.C. Perruchoud, *Factors Influencing the Carboxy- and Air-Reactivity Behavior of Prebaked Anodes in Hall--Heroult Cells* in *TMS*. 1986: New Orleans, USA. p. 575-580.
2. Houston, G.J. and H.A. Øye, *Consumption of Anode Carbon During Aluminium Electrolysis.* Aluminium, 1985. 61(I-III).
3. Marie-Josée-Chollier, A.G., et al., *Anode reactivity: effect of coke calcination level.* Light Metals, 2009: p. 905-908.
4. Lhuissier, J., et al., *Use of under-calcined coke for the production of low reactivity anodes.* Essential Readings in Light Metals: Electrode Technology for Aluminum Production, Volume 4, 2013: p. 109-113.
5. Fischer, W.K. and R. Perruchoud. *Influence of coke calcining parameters on petroleum coke quality*. in *Light Metals 1985. Proceedings of the Technical Sessions at the 114th Annual Meeting of the Metallurgical Society of AIME.* 1985. New York, NY, USA: Metallurgical Soc of AIME.
6. Engvoll, M.A., H.A. Oye, and M. Srlie. *Influence of bath contaminations on anode reactivity*. in *Light Metals 2001, February 11, 2000 - November 15, 2000*. 2001. New Orleans, LA, United states: Minerals, Metals and Materials Society.
7. Müftüoglu, T., B. Steine, and R. Fernandez, *Anode Burning Behaviour and Sodium Sensitivity of Coke from Different Feedstocks: A Pilot Scale Study.* Light Metals 1993, 1993: p. 543-548.
8. Müftüoglu, T. and H. Øye, *Reactivity and electrolytic consumption of anode carbon with various additives.* Essential Readings in Light Metals: Electrode Technology for Aluminum Production, Volume 4, 1987: p. 667-671.
9. Rolle, J.G. and Y.K. Hoang, *Studies of the impact of vanadium and sodium on the air reactivity of coke and anodes.* Essential Readings in Light Metals: Electrode Technology for Aluminum Production, Volume 4, 1995: p. 606-610.
10. Rolle, J.G. and R.A. Czikall. *Use of coke air reactivity testing for predicting anode air reactivity*. in *Light Metals 2001, February 11, 2000 - November 15, 2000*. 2001. New Orleans, LA, United states: Minerals, Metals and Materials Society.
11. Buhler, U. and R.C. Perruchoud, *Dynamic process optimization.* LIGHT MET(WARRENDALE PA), 1995: p. 707-714.
12. Lustenberger, M., *Heat treatment of anodes for the Aluminium Industry*, in *Institut des matériaux*. 2004, Faculté Sciences et Techniques de l'Ingénieur: Lausanne, Switzerland. p. 143.
13. Coste, B. and J. Schneider, *Influence of coke real density on anode reactivity consequence on anode baking.* Light Metals 1994, 1994: p. 583-591.
14. Foosnæs, T., et al., *Measurement and control of the calcining level in anode baking furnaces.* Essential Readings in Light Metals: Electrode Technology for Aluminum Production, Volume 4, 1995: p. 418-421.
15. Fischer, W.K., et al., *Baking parameters and the resulting anode quality.* Essential Readings in Light Metals: Electrode Technology for Aluminum Production, Volume 4, 1993: p. 427-433.
16. Edwards, L., et al., *Use of shot coke as an anode raw material.* Essential Readings in Light Metals: Electrode Technology for Aluminum Production, Volume 4, 2013: p. 36-41.
17. Schmidt-Hatting, D.W., A. Kooijman, and R. Perruchoud, *Investigation of the quality of recycled anode butts.* Essential Readings in Light Metals: Electrode Technology for Aluminum Production, Volume 4, 1990: p. 251-266.
18. Rey Boero, J.F., *Studies on anode reactivity to oxidant gases.* AIME, 1980: p. 441-458.

19. Kuang, Z.-l., et al., *Effect of baking temperature and anode current density on anode carbon consumption.* Metallurgical and Materials Transactions B, 1996. 27(2): p. 177-183.
20. Edwards, L., *The History and Future Challenges of Calcined Petroleum Coke Production and Use in Aluminum Smelting.* JOM, 2015. 67(2): p. 308-321.
21. Tkac, M., *Porosity Development in Composite Carbon Materials during Heat Treatment*, in *Department of Materials Science and Engineering*. 2007, Norwegian University of Science and Technology: Trondheim. p. 189.
22. Suriyapraphadilok, U., et al., *Physical, chemical and X-Ray Computed Tomography characterization of anode butt cores.*
23. Bird, N., B. McEnaney, and B.A. Sadler. *Some practical consequences of analyses of the carboxy and airburn reactions of anode carbons*. in *Proceedings of the 119th TMS Annual Meeting, February 18, 1990 - February 22, 1990*. 1990. Anaheim, CA, USA: Publ by Minerals, Metals & Materials Soc (TMS).
24. Turkdogan, E.T., R. Olsson, and J. Vinters, *Pore characteristics of carbons.* Carbon, 1970. 8(4).
25. Tran, K.N., S.K. Bhatia, and A. Tomsett, *Air Reactivity of Petroleum Cokes: Role of Inaccessible Porosity.* Industrial & Engineering Chemistry Research, 2006. 46(10): p. 3265-3274.
26. Tordai, T., *Anode dusting during the electrolytic production of aluminium*. 2007, École Polytechnique Fédérale de Lausanne. p. 351.
27. Chevarin, F., et al., *Effects of Microstructural Characteristics on Anode Reactivity*, in *COM-2011, 40th Annual Conference of Metallurgists of CIM*, M.F.e. al, Editor. 2011: Montréal, Canada.
28. Azari, K., et al. *Influence of mixing parameters on the density and compaction behavior of carbon anodes used in aluminum production*. in *Advanced Materials Research*. 2012: Trans Tech Publ.
29. Azari, K., et al., *Compaction properties of carbon materials used for prebaked anodes in aluminum production plants.* Powder Technology, 2013. 246(0): p. 650-657.
30. Azari, K., ed. *Investigation of the materials and paste relationship to improve forming process and anode quality*. Ph.D Thesis. 2013, Laval University, Canada.
31. Hussein, A., et al., *Effects of heat treatment and acid washing on properties and reactivity of charcoal.* Biomass and Bioenergy, 2016. 90: p. 101-113.
32. Chevarin, F., et al. *Air and CO_2 Reactivity of Carbon Anode and Its Constituents: An Attempt to Understand Dusting Phenomenon*. in *Light Metals 2015*. Orlando, United States.
33. Chevarin, F., et al., *Active pore sizes during the CO_2 gasification of carbon anode at 960 °C.* Fuel, 2016. X(X): p. X-X.
34. Chevarin, F., et al., *Characterization of carbon anode constituents under CO 2 gasification: a try to understand the dusting phenomenon.* Fuel, 2015. 156: p. 198-210.
35. Tran, K.N., et al., *Crystalline Structure Transformation of Carbon Anodes during Gasification.* Energy & Fuels, 2008. 22(3): p. 1902-1910.
36. Chevarin, F., et al., *Substrate effect of coke particles on the structure and reactivity of coke/pitch mixtures in carbon anodes.* Fuel, 2016. 183: p. 123-131.
37. D'amore, M., L. Tognotti, and A. Sarofim, *Oxidation rates of a single char particle in an electrodynamic balance.* Combustion and flame, 1993. 95(4): p. 374-382.
38. Boero, J.R., *The reaction of petroleum cokes with air.* Carbon, 1987. 25(4): p. 477-483.
39. Bhatia, S.K. and D.D. Perlmutter, *A random pore model for fluid-solid reactions: I. Isothermal, kinetic control.* AIChE Journal, 1980. 26(3): p. 379-386.
40. Ballal, G. and K. Zygourakis, *Evolution of pore surface area during noncatalytic gas-solid reactions. 2. Experimental results and model validation.* Industrial & engineering chemistry research, 1987. 26(9): p. 1787-1796.

41. ISO15901-1, *Pore size distribution and porosity of solid materials by mercury porosimetry and gas adsorption -- Part 1: Mercury porosimetry* 2005.
42. Hume, S.M., et al. *Model for petroleum coke reactivity*. in *TMS*. 1993. Denver, CO, USA.
43. Farr-Wharton, R., et al., *Chemical and electrochemical oxidation of heterogeneous carbon anodes.* Electrochimica Acta, 1980. 25(2): p. 217-221.
44. Chevarin, F., et al., *Active pore sizes during the CO 2 gasification of carbon anode at 960° C.* Fuel, 2016. 178: p. 93-102.